

# Aging and Ball-Milling as Low-Energy and Environmentally Friendly Methods for the Synthesis of Pd(II) Photosensitizers

Marina Juribašić,<sup>†</sup> Ivan Halasz,<sup>†</sup> Darko Babić,<sup>†</sup> Dominik Cinčić,<sup>‡</sup> Janez Plavec,<sup>§</sup> and Manda Čurić\*<sup>†</sup>

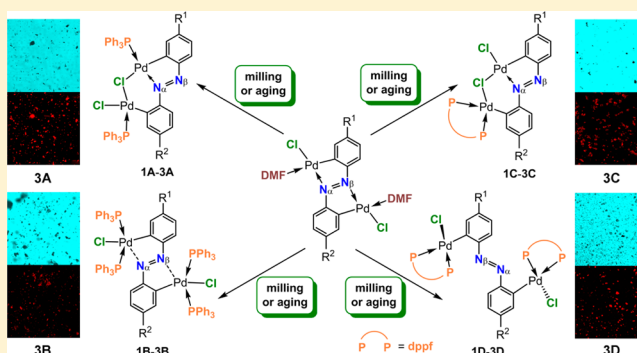
<sup>†</sup>Ruder Bošković Institute, Bijenička 54, HR-10002 Zagreb, Croatia

<sup>‡</sup>Department of Chemistry, Faculty of Science, University of Zagreb, Horvatovac 102a, HR-10000 Zagreb, Croatia

<sup>§</sup>Slovenian NMR Centre, National Institute of Chemistry, Hajdrihova 19, SI-1000 Ljubljana, Slovenia

## S Supporting Information

**ABSTRACT:** Simple and efficient solid-state synthetic methods, aging and ball milling (liquid-assisted grinding, LAG), have been employed to achieve reactions of triphenylphosphine (tpp) and 1,1'-bis(diphenylphosphino)ferrocene (dppf) with dicyclopalladated azobenzenes (DMF)-PdCl( $\mu$ -R<sup>1</sup>C<sub>6</sub>H<sub>3</sub>N=NC<sub>6</sub>H<sub>3</sub>R<sup>2</sup>)PdCl(DMF), R<sup>1</sup> = H, OCH<sub>3</sub>, N(CH<sub>3</sub>)<sub>2</sub> and R<sup>2</sup> = H, NO<sub>2</sub>. For the first time the aging processes have been applied in the formation of Pd(II) heteroleptic complexes. Both synthetic procedures lead to four types of tetra- or pentacoordinated complexes (tpp)PdCl{( $\mu$ -Cl)( $\mu$ -R<sup>1</sup>C<sub>6</sub>H<sub>3</sub>N=NC<sub>6</sub>H<sub>3</sub>R<sup>2</sup>)}Pd(tpp) **1A–3A**, (tpp)<sub>2</sub>PdCl-( $\mu$ -R<sup>1</sup>C<sub>6</sub>H<sub>3</sub>N=NC<sub>6</sub>H<sub>3</sub>R<sup>2</sup>)PdCl(tpp)<sub>2</sub> **1B–3B**, PdCl{( $\mu$ -Cl)( $\mu$ -R<sup>1</sup>C<sub>6</sub>H<sub>3</sub>N=NC<sub>6</sub>H<sub>3</sub>R<sup>2</sup>)}Pd(dppf) **1C–3C**, and (dppf)-PdCl( $\mu$ -R<sup>1</sup>C<sub>6</sub>H<sub>3</sub>N=NC<sub>6</sub>H<sub>3</sub>R<sup>2</sup>)PdCl(dppf) **1D–3D**, in which azobenzenes simultaneously act as monodentate C- and bidentate C,N-donors (**A**, **B**, and **C** complexes) or, for the first time, only as double C-donors (**D** complexes). Although their formation requires complex intramolecular transformations, aging and ball milling have been proved to be efficient synthetic methods. All products have been fully characterized in solid state and solution. Solid-state structures of complexes have been resolved by a single crystal or powder X-ray diffraction (PXRD) and solid-state NMR spectroscopy. Their electronic structures have been rationalized by the quantum-chemical calculations. The structural features of complexes and their stability in solutions have been evaluated by <sup>1</sup>H and <sup>31</sup>P NMR spectroscopy along with the ESI-MS spectrometry. The absorption and emission properties of complexes have been studied, and the nature of their electronic transitions in the low energy region has been examined by TD-DFT calculations. Significant fluorescence observed for the complexes with 4-dimethylamino-4'-nitroazobenzene ligand at room temperature in solid state and/or in the solution makes them interesting for potential applications as photoactive units in optical devices.



## INTRODUCTION

During the past decade mechanochemical reactions are becoming increasingly popular preparative methods with applications in the synthesis of inorganic, organic, coordination, and supramolecular compounds.<sup>1</sup> Consequently, a large number of papers and reviews has been published over the past several years dealing with synthetic and mechanistic aspects of these reactions.<sup>2</sup> Mechanochemical reactions induced by grinding (neat grinding, NG; liquid-assisted grinding, LAG; or ion and liquid-assisted grinding, ILAG) of the solid reactants are often faster and more selective than solvent-based or solvothermal reactions.<sup>3</sup> Furthermore, the complete absence of solvent or its use in only catalytic amounts results in reduced environmental pollution and renders mechanochemical preparative methods relevant for industrial and pharmaceutical applications.<sup>4</sup> However, solid-state reactions can also occur without an input of mechanical energy.<sup>5</sup> The mixture of solid reactants will undergo a chemical reaction in particular if exposed to solvent vapors. These processes known as

accelerated aging and vapor digestion<sup>5</sup> are extremely simple and require minor energy input, while they may be quantitative. Despite these advantages, preparations of compounds by aging are still rare.

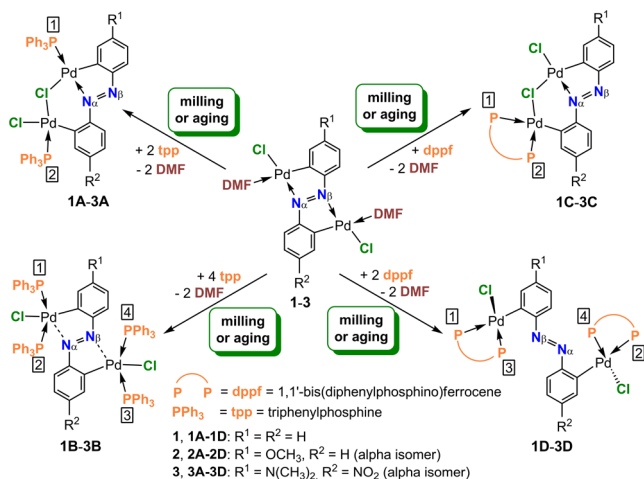
We have decided to investigate aging reactions in the synthesis of heteroleptic Pd(II) complexes because of their specific advantages described above. Recently, we have mechanochemically prepared the first examples of Pd(II) heteroleptic complexes with triphenylphosphine and azobenzenes.<sup>6</sup> The solid-state synthetic route produced monochloride-bridged complexes and demonstrated that complex structural changes are feasible during the synthesis in solid state.<sup>6</sup> As an extension of this work, here we report on the synthesis of a series of new organopalladium complexes containing azobenzenes and triphenylphosphine (tpp) or 1,1'-bis-

Received: January 7, 2014

Published: February 24, 2014

(diphenylphosphino)ferrocene (dppf) by two solid-state synthetic routes: aging and ball milling, Scheme 1.

Scheme 1



In addition to the synthetic objectives, we have also focused on the structural as well as the photophysical properties of the new complexes because of their potential application in light-emitting devices and as photochemical catalysts.<sup>7</sup> Although phosphine ligands are among the most frequently used ligands in the palladium chemistry,<sup>8</sup> investigations of the photophysical properties of Pd(II) complexes containing both azobenzene and phosphine moieties have not been reported yet. Our previous studies of dicyclopalladated azobenzenes have demonstrated a strong effect of 4,4'-substituents in azobenzene unit on their photophysical properties, which may be additionally enhanced by a suitable ancillary ligand.<sup>9</sup> The influence of the triphenylphosphine and 1,1'-bis(diphenylphosphino)ferrocene as ancillary ligands on the photophysical properties of the dipalladated azobenzenes was examined by absorption and emission spectroscopy as well as by theoretical calculations.

## RESULTS AND DISCUSSION

**Synthesis and Characterization.** The synthetic routes to four series of heteroleptic Pd(II) complexes are described in Scheme 1. Reactions of tpp and dppf with initial compounds in molar ratio 2:1 and 1:1 lead to the Cl-bridged 1A–3A and 1C–3C complexes, respectively, in which azobenzenes simultaneously act as monodentate C- and bidentate C,N-donors. When the molar ratio of phosphine ligand and dicyclopalladated azobenzenes was 4:1 (tpp) or 2:1 (dppf), the reactions resulted in 1B–3B or 1D–3D complexes, respectively. For the first time, in D complexes azobenzene acts as the double C-donor, while in B complexes it has the same coordination mode as in A and C complexes. All products are air-stable solids, A and C complexes are soluble in solvents with poor coordinating ability, i.e.,  $\text{CHCl}_3$ ,  $\text{CH}_2\text{Cl}_2$ , or  $(\text{CH}_3)_2\text{CO}$ , while B and D complexes are only sparingly soluble. Except 3A and C complexes, all the others are insoluble in solvents with coordinating ability, i.e., DMSO, DMF, or  $\text{CH}_3\text{CN}$ .

All compounds were obtained by aging in acetone vapors and by liquid-assisted grinding (LAG) using catalytic amount of acetone or nitromethane at room temperature. The mixing of solid reactants in the aging reactions was done by gentle grinding in an agate mortar in order to avoid mechanical

activation. PXRD of such treated reactants did not detect the presence of new products. All solid-state reactions are characterized by a drastic color change and almost quantitative yields. Compared to mechanochemical reactions, which were complete within 30–90 min and used 30  $\mu\text{L}$  of solvent, aging reactions lasted up to 72 h and required about 1 mL of solvent. Both methods yield pure products; however collecting of the products from reaction vessels introduces small mass losses, lowering the isolated yields to about 88 and 98% for mechanochemical and aging reactions, respectively.

The purity of the bulk products was determined by PXRD. PXRD patterns of aging and LAG products were compared, and for complexes 1A, 3A, 1C, and 1D–3D, these pairs are in good agreement, Figures 1 and S1–S12, Supporting

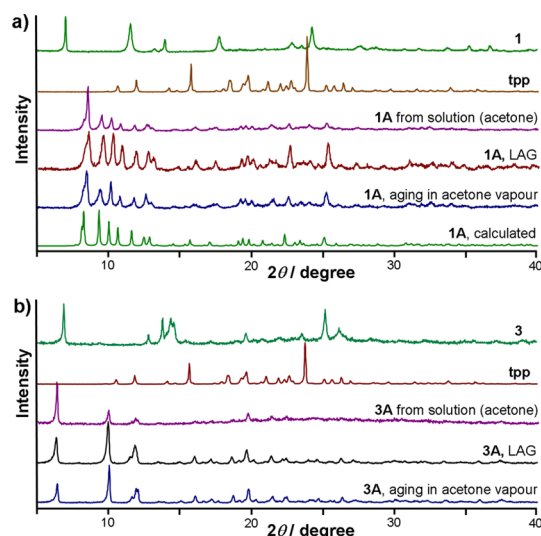


**Figure 1.** PXRD patterns of complexes (a) 1A and (b) 3A involving reactants tpp, 1 and 3.

Information. Differences between the remaining pairs of PXRD patterns were rationalized in terms of a large number of different possible conformers as indicated by the quantum chemical calculations.

In order to identify the aging and LAG species, the single crystals of 1A–3A and 3B were isolated from acetone or acetone–ethanol mixture by recrystallization, and analogous solvent-based reactions were carried out in acetone; see the Supporting Information. The results of X-ray structural analysis, solid-state and solution  $^{31}\text{P}$  NMR spectra as well as ESI mass spectra and PXRD have confirmed that the aging and LAG reactions lead to the same types of complexes.

The formation of A and C complexes requires the substitution of DMF with tpp or dppf, *cis*–*trans* isomerization of donor atoms with respect to Pd–C bond and breaking of only one Pd–N bond, which allows the rotation of one phenyl ring and positioning of both palladium atoms on the same side of azobenzene in order to form a Cl-bridge. Prerequisites for the formation of B and D complexes are also the exchange of DMF with tpp or dppf, *cis*–*trans* isomerization, and in the cases of D products, the breaking of both Pd–N bonds and the rotation of both phenyl rings with bulky substituents, Scheme 1.

**NMR Spectra.**  $^{31}\text{P}$  NMR spectra of A and C complexes recorded in  $\text{CHCl}_3$  contain two signals (two sets for 2A and 2C), confirming that two phosphorus atoms of each phosphine

ligand (tpp and dppf) are nonequivalent, Figure 2. A double set of signals in the ratio 3:1 observed in the  $^{31}\text{P}$  NMR as well as in

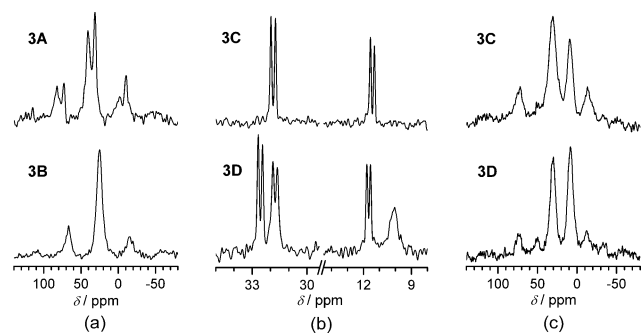


**Figure 2.**  $^{31}\text{P}$  NMR spectra of (a) **3A** and **3B** (MAS); (b) **3C** and **3D** ( $\text{CDCl}_3$ ); (c) **3C** and **3D** (MAS).

$^1\text{H}$  NMR spectra of **2A** and **2C** complexes is due to the presence of alpha and beta isomers formed by breaking either the  $\text{Pd}-\text{N}_\alpha$  or the  $\text{Pd}-\text{N}_\beta$  bond,<sup>6</sup> Scheme 1, Table S1, and Figure S13 (Supporting Information). The signals in the spectra of **C** complexes are split into doublets due to the P–P coupling ( $^2J_{\text{PP}}$  about 30 Hz), indicating chelate binding mode of dppf ligand.<sup>10</sup> The solid-state  $^{31}\text{P}$  NMR spectra of the **A** and **C** complexes contain two broad signals, and consequently, it is not possible to see the difference between the alpha and beta isomers as well as the splitting of the phosphorus signals of the **C** complexes.

The  $^{31}\text{P}$  NMR spectra confirmed the same coordination mode of dppf ligands in **C** and **D** complexes. The spectrum of complex **1D** contains two doublets with  $^2J_{\text{PP}}$  about 30 Hz, while the complexes of asymmetrically substituted azobenzenes (**2D** and **3D**) with two nonequivalent phenyl rings contain four signals, Figure 2 and Table S1 (Supporting Information). These results indicate that each Pd atom in **D** complexes is bonded to one dppf molecule. The spectra of complexes **2D** and **3D** recorded in the solid state contain two broad signals due to small differences between chemical shifts of atoms P1 and P2 as well as P3 and P4, Scheme 1.

The solid-state  $^{31}\text{P}$  NMR spectra of the **B** complexes contain only one phosphorus signal suggesting very similar environment around four phosphorus atoms, Figure 2 and Table S1 (Supporting Information). However, the spectra recorded in  $\text{CHCl}_3$  have revealed that in the solution the **B** complexes transform into the thermodynamically more favorable **A** complexes, Figure S14 (Supporting Information). Their spectra recorded immediately after dissolving in  $\text{CHCl}_3$  contain one singlet corresponding to **B** complex at about 29 ppm, two singlets of **A** complex, and one broad signal of free tpp ligand. The **B** complexes transform completely into **A** complexes within 24 h in solution, Figure S14 (Supporting Information). Such transformations are also supported by the quantum-chemical calculations as well as by ESI-MS and UV–vis spectra. The **A** complexes transform back to **B** during evaporation of the solvent accompanied by precipitation.

**Mass Spectra.** The ESI-MS spectra of all complexes were recorded shortly after their dissolving. Base peaks of fresh solutions of **A**, **C**, and **D** complexes corresponded to  $[\text{M}-\text{Cl}]^+$  ions (Figures 3 and 4). The assignment was additionally supported by comparing the experimental peaks with the calculated isotopic patterns, thus confirming the formulation of these complexes.

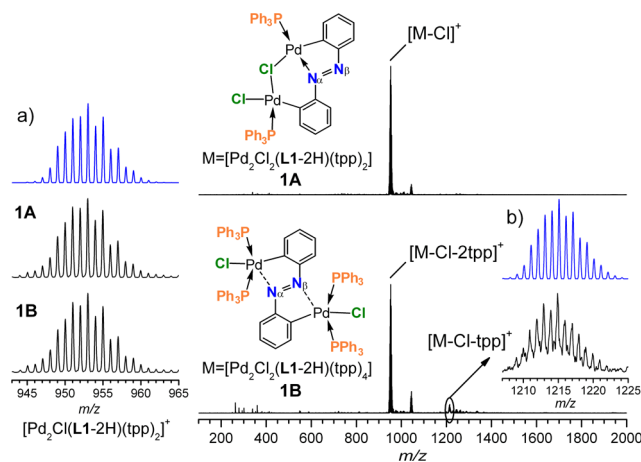


**Figure 3.** (+)ESI mass spectra of **1A** and **1B** in  $\text{CHCl}_3/\text{MeOH}$  recorded 3 min after dissolving. Insets: Experimental (black) and calculated (blue) isotopic pattern of peaks assigned to (a)  $[\text{Pd}_2\text{Cl}(\text{L1-2H})(\text{tpp})_2]^+$  ( $\text{C}_{48}\text{H}_{38}\text{N}_2\text{P}_2\text{Pd}_2\text{Cl}$ ) and (b)  $[\text{Pd}_2\text{Cl}(\text{L1-2H})(\text{tpp})_3]^+$  ( $\text{C}_{66}\text{H}_{53}\text{N}_2\text{P}_3\text{Pd}_2\text{Cl}$ ).

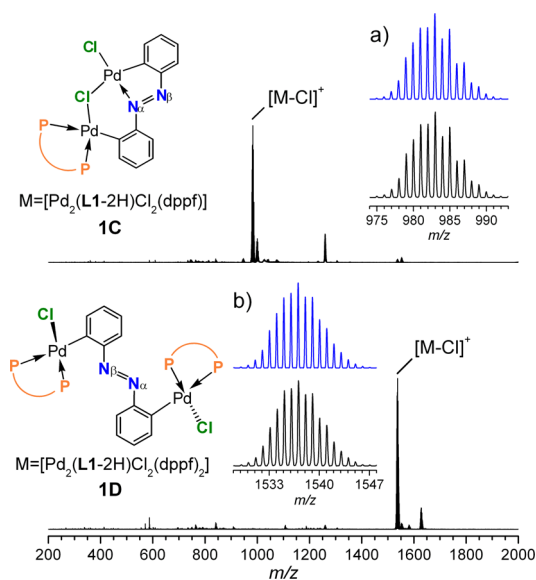


**Figure 4.** (+)ESI mass spectra of **1C** and **1D** in  $\text{CHCl}_3/\text{MeOH}$  recorded 3 min after dissolving. Insets: Experimental (black) and calculated (blue) isotopic pattern of peaks assigned to  $[\text{Pd}_2\text{Cl}(\text{L1-2H})(\text{dppf})_2]^+$  ( $\text{C}_{46}\text{H}_{36}\text{N}_2\text{P}_2\text{Pd}_2\text{FeCl}$ ) and  $[\text{Pd}_2\text{Cl}(\text{L1-2H})(\text{dppf})]^+$  ( $\text{C}_{80}\text{H}_{64}\text{N}_2\text{P}_4\text{Pd}_2\text{Fe}_2\text{Cl}$ ).

In the spectra of **B** complexes, peaks assigned to  $[\text{M}-\text{Cl}-\text{tpp}]^+$  ions were the highest in mass, indicating that these complexes readily decompose in solution, Figure 3. Species  $[\text{M}-\text{Cl}-2\text{tpp}]^+$  that correspond in mass to  $[\text{M}-\text{Cl}]^+$  ions of **A** complexes were assigned as the base peaks, Figure 3. After one day, the spectra of the solution of **B** complexes contained many unaccountable peaks that were not observed in the spectrum of the fresh solution, Figure S14 (Supporting Information). It is interesting to note here that after collisional activation the fragmentation of the **A** (and **B**) complexes yields almost exclusively  $\text{PPh}_4^+$  ion ( $m/z$  339), Scheme S1 (Supporting Information). This can be explained by the breaking of the P–C bond in one tpp ligand, phenyl group migration from one palladium atom to another, bonding to the second tpp and elimination of the  $\text{PPh}_4^+$  ions. Similar behavior was observed for the mononuclear Pd

complexes with  $\text{tpp}^{11}$  but was not reported using compounds with two closely positioned Pd atoms that can communicate and exchange ligands. The interchange between phosphorus bound aryl groups is a pitfall of many palladium-mediated catalytic reactions, and more information about these processes is needed.<sup>11</sup> Fragmentation of **C** and **D** complexes leads to the breaking of the bond with  $\text{dppf}$  ligand and to the elimination of the ferrocenyl or phenyl moieties, Scheme S2 (Supporting Information).

**Crystal Structures.** Molecular structures of complexes resolved by single-crystal (**2A** and **3B**) or powder X-ray diffraction (**1D**) are shown in Figures 5, 6, and S17

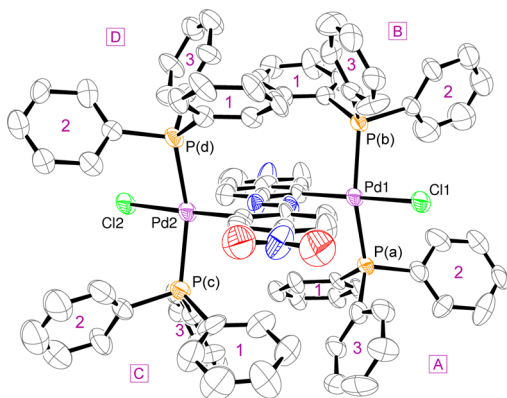


**Figure 5.** Molecular structure of **3B**. Displacement ellipsoids are drawn at 30% probability level. Hydrogen atoms are omitted,  $\text{tpp}$  ligands are labeled A–D and phenyl rings are numbered 1 (rings with atoms C1a–C6a, C1b–C6b, C1c–C6c, C1d–C6d), 2 (rings with atoms C7a–C12a, C7b–C12b, C7c–C12c, C7d–C12d) and 3 (rings with atoms C13a–C18a, C13b–C18b, C13c–C18c, C13d–C18d) for clarity.

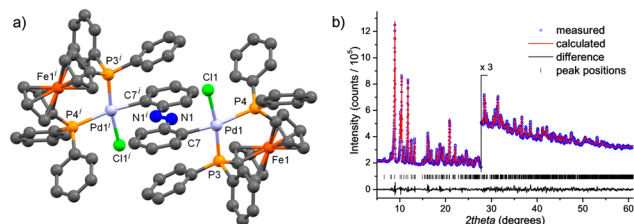


**Figure 6.** (a) Molecular structure of **1D**. Hydrogen atoms are omitted for clarity. Sym. op.  $i$  is  $[1 - x, 1 - y, 2 - z]$ . (b) Final Rietveld refinement plot for **1D**. The high-angle region above approximately  $28^\circ$  is enlarged to reveal more detail.

(Supporting Information), and the selected bonds and angles are presented in Table S2 (Supporting Information). All attempts to obtain single crystals of **C** and **D** complexes were unsuccessful, and these complexes were structurally characterized by PXRD. The results of the X-ray structural analysis have confirmed the coordination mode of azobenzenes and phosphines as well as approximately square planar coordination of Pd atoms in **A** and **D** complexes and pseudotrigonal-bipyramidal coordination in **B** complexes.

Two palladium centers in the complex **3B** are bridged by the azobenzene ligand, and each of them is pentacoordinated by the carbon atom of the phenyl ring, the azo-nitrogen, the chloride ion and two phosphorus atoms of  $\text{tpp}$  ligands, which are mutually in *trans* position, Figure 5.

Two  $\text{tpp}$  molecules are *cis* with respect to Pd–C bond, while both chlorides are oriented *trans* to Pd–C bond in contrast to their *cis* position in the initial compound **3**. Molecular structure of **3B** complex is characterized by the planarity of the azobenzene skeleton, Pd and Cl atoms. Pd centers are pentacoordinated with the Pd–N distances of 2.608(13) and 2.630(11) Å. This complex is one of the rare examples of pentacoordinated Pd(II) compounds.<sup>12</sup> Complex **3B** packs in layers in the  $xy$ -plane with numerous C–H $\cdots$ Cl interactions, Figure S15 (Supporting Information). Weak C–H $\cdots$ O=N interactions between dimethylamino- and nitro-groups connect these layers in the  $[001]$  direction.

Crystal and molecular structure of **1D** complex was solved by simulated annealing in direct space by using various candidate molecular structures provided by quantum-chemical calculations. The calculations involved both isomers, with and without Pd–N coordination. In this crystal structure, the molecule was found to have the center of symmetry bisecting the N=N bond of the azobenzene fragment. Palladium atoms are in square-planar coordination environment with two phosphorus atoms, the chloride and the azobenzene carbon as donors, confirming the breaking of both Pd–N bonds in initial compound **1**, Figure 6a. Two phosphorus atoms of  $\text{dppf}$  molecule are mutually *cis*, since  $\text{dppf}$  acts as a bidentate ligand in **D** complexes. Consequently, one of the phosphorus atoms is oriented *trans* to the Pd–C bond, Scheme 1 and Figure 6a. The azobenzene skeleton and Pd atoms also have almost planar arrangement in **1D** complex. Furthermore, measured and calculated PXRD patterns show a very good agreement, Figure 6b. The molecular structure of this compound is probably among the most complex structures of coordination compounds solved by PXRD.

Despite the crystal's low quality, the single crystal X-ray diffraction data of **2A** were sufficient to identify it as the Cl-bridged complex in which 4-methoxyazobenzene simultaneously acts as the monodentate C- and bidentate C,N-donor. Its molecular structure, which is analogous to recently reported structures **1A** and **3A**,<sup>6</sup> has confirmed breaking of only one Pd–N bond in the initial compound **2**, Figure S16 (Supporting Information). Pd centers in **A** complexes are bridged by the azobenzene and additionally by the Cl-bridge. Pd(1) atom of **A** complexes is coordinated by carbon, azo-nitrogen, bridged chloride, and phosphorus. Pd(2) atom is bonded to carbon, terminal chloride, bridged chloride, and phosphorus. Both  $\text{tpp}$  ligands are oriented *cis* to the Pd–C bond as in complex **3B**. The structures of **A** complexes are characterized by the intramolecular metal–metal interactions. The Pd $\cdots$ Pd distances in **A** complexes are slightly shorter (about 0.15 Å) than the sum of their van der Waals radii. Furthermore, despite the low quality of the X-ray data, two molecules of **2A**, alpha and beta isomers, were unambiguously found in the asymmetric unit, Figure S16 (Supporting Information), confirming the presence of both isomers. This is in a good agreement with NMR studies. In addition, ethanol molecules were found in two accessible voids in the crystal packing. Each of two isomeric molecules of **2A** complex forms a layer in  $xy$  plane, Figure S17 (Supporting Information). These two layers are repeated along the  $[001]$  direction.

We also attempted to solve the crystal structure of **1C** but were not successful. The sample was of poorer crystallinity than that of **1D** leading to less well resolved peaks and weak scattering at higher diffraction angles, which hindered structure solution, Figure S18 (Supporting Information). However, we

were able to index the powder diffraction pattern (Table S3, Supporting Information) and found that one-quarter of the unit cell volume corresponded very well to the estimated volume of one molecule of **1C**. This strongly indicated that the assumed molecular structure, as given in Scheme 1, is correct. On the basis of the presented results, spectral data and recently reported molecular structures of the complexes of dipalladated azobenzenes with bidentate 2,2-bipyridine as well as the results of quantum-chemical calculations, the structures of **C** complexes can be presumed with a great certainty to be similar to those of **A** complexes as given in Scheme 1.

Finally, the results of the X-ray structural analysis have revealed *cis*–*trans* isomerism in isolated complexes and also that the bond lengths between Pd atom and coordinated atoms in *trans* position are significantly longer than could be predicted on the basis of their covalent radii because of a strong *trans* influence of C and P donors, which is also confirmed by quantum-chemical calculations.<sup>13</sup>

**Quantum-Chemical Calculations.** Because of two labile bonds around Pd atoms in the initial compounds, the considered complexes may exist in several isomeric forms. As we recently reported,<sup>6</sup> the reactions of initial complexes **1**–**3** and tpp ligand in 1:2 molar ratio could result in two isomers (denoted as **A** and **A'**, Scheme S4, Supporting Information), which differ in the coordination mode of azobenzenes. Besides, each isomer can have *cis* or *trans* orientation of tpp ligand with respect to the Pd–C bond. Furthermore, **A** isomers of asymmetrically substituted azobenzenes may exist as alpha and beta isomers formed by breaking either the Pd–N<sub>α</sub> or the Pd–N<sub>β</sub> bond (see NMR section). However, the relative Gibbs energies have shown that isolated isomers **1A**–**3A** are the most stable, Table S5 (Supporting Information).

It was noted that **1B**–**3B** complexes dissolved in CHCl<sub>3</sub> transform to **1A**–**3A** complexes by releasing two tpp molecules. Calculated Gibbs energies of **1A**–**3A** complexes are lower than those of **1B**–**3B** complexes by 11–12 kcal/mol, which is in agreement with the experimental findings. Since **1B** complex may have an inversion center as the symmetry element, we have optimized C<sub>i</sub> geometry to compare its Gibbs energy with the conformer determined by the X-ray diffraction. To our surprise, the conformer with C<sub>i</sub> symmetry was calculated to have lower Gibbs energy than the experimental conformer by 5.6 kcal/mol. Similar findings were obtained with **2B** and **3B** complexes (6.9 and 6.3 kcal/mol). The fact that seemingly less stable conformers were isolated can be attributed to the unaccounted solid state effects. Since the crystal and molecular structures of **1C**–**3C** complexes were not resolved by single-crystal or powder X-ray diffraction, their geometries were tentatively assigned from the most stable calculated conformers. Eight conformers were found for each of the three species, with the Gibbs energies of those less stable being 0.6–9 kcal/mol higher than of the most stable conformer (geometries and energies of all conformers are listed in Supporting Information). The geometries of the most stable conformers were used for the calculation of UV–vis and NMR spectra.

**Absorption and Emission Spectra.** The UV–vis spectral data for complexes **1A**–**3A**, **1C**–**3C**, and **1D**–**3D** recorded in CHCl<sub>3</sub> at room temperature are summarized in the Supporting Information. The spectra of **B** complexes could not be obtained because of their transformation into **A** complexes. The experimental absorption bands corresponding to the singlet excited states are assigned on the basis of TD-DFT calculations, Figures 7 and S19–S25 (Supporting Information). The first 10

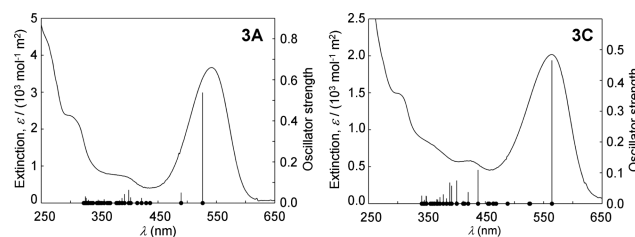


**Figure 7.** UV–vis spectra of **3A** and **3C** recorded in CHCl<sub>3</sub>. Vertical lines denote calculated transitions from the ground to the excited singlet states; the size of vertical lines is proportional to the calculated oscillator strengths.

calculated excited states represented by the electronic transition with the largest contribution are listed in Tables S6–S8 (Supporting Information). The calculated transition intensity is well while the calculated wavelengths are slightly red or blue-shifted relative to experimental values for these transitions. According to calculations, the most intense bands in the complexes **1A**–**3A**, **1C**–**3C**, and **1D**–**3D** are assigned as intraligand (IL)  $\pi^* \leftarrow \pi$  transitions localized on the azobenzene ligands. As expected, these transitions have higher intensity and are significantly shifted to the lower energies in complexes with 4-dimethylamino-4'-nitroazobenzene **3A**, **3C**, and **3D** than their analogues with azobenzene and 4-methoxyazobenzene, Figures 7 and S20–S25 (Supporting Information). Furthermore, the less intense transitions in **A** and **C** complexes have metal to ligand (MLCT), metal-chloride to ligand (MXLCT), metal–metal to ligand (MMLCT) and long-range ligand to ligand (L'LCT) charge transfer character, where M = Pd, L = azobenzene ligand, X = terminal or bridging chloride and L' = tpp or dppe, Tables S6–S8 (Supporting Information). Compared to **D** complexes, the majority of the transitions in **A** and **C** complexes have mixed character involving one or more above-described charge transfers with varying contribution  $\pi^* \leftarrow \pi$  intraligand transitions.

The complexes with 4-dimethylamino-4'-nitroazobenzene fluoresce at room temperature in the low energy region in solid state (**3A**, **3B**, **3C**, and **3D**) and in the solution (**3A**, **3C**, and **3D**), confirming the combined influence of the electron-donating and electron-withdrawing 4,4'-substituents on the fluorescence of dipalladated azobenzenes, Table 1, Figures 8 and S25 (Supporting Information). In addition, the presence of phosphine ligands significantly increases intensity of their fluorescence, which is the most pronounced for the bridged complex **3A**. Its emission is even much more intense than that

**Table 1.** Fluorescence Data

	$\lambda_{\text{exc}}$ (nm)	$\lambda_{\text{em}}$ (nm)	
<b>3A</b>	580	615	CHCl <sub>3</sub>
	543	610–660	solid
	633	610–660	
<b>3B</b>	–	–	CHCl <sub>3</sub>
	594	610–600	solid
	633	650–700	
<b>3C</b>	570	635	CHCl <sub>3</sub>
	594	630–660	solid
	633	640–680	
<b>3D</b>	580	632	CHCl <sub>3</sub>
	594	640–610	solid
	633	640–610	

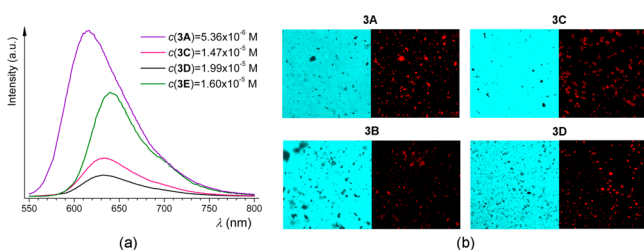


**Figure 8.** Fluorescence of 4-dimethylamino-4'-nitroazobenzene complexes in (a)  $\text{CHCl}_3$  ( $\lambda_{\text{exc}} = 580$  nm for 3A, 3D, 3E and  $\lambda_{\text{exc}} = 570$  nm for 3C) and (b) the solid state ( $\lambda_{\text{exc}} = 633$  nm). The emission intensity is normalized to the same concentration.

of the complex with 4-dimethylamino-4'-nitroazobenzene and 2,2'-bipyridine reported recently (denoted as 3E in Figure 8).

The complexes 3A, 3C, and 3D exhibit fluorescence in the  $\text{CHCl}_3$  solution with  $\lambda_{\text{max}}$  at 615, 635, and 632 nm upon excitation at 580, 570, and 580 nm, respectively. Spectra of these complexes are similar in terms of their band shapes and its position, indicating that the same emissive state is involved in each case. According to the literature observed emission can be attributed to IL  $\pi^* \rightarrow \pi$ , MLCT, or MMLCT transitions.<sup>14</sup> The fluorescence emission was also observed in the solid-state with a confocal microscope for complexes 3A, 3B, 3C, and 3D in the wavelength range 600–700 nm upon excitation at 543 and 633 nm for 3A complex (Figure S29, Supporting Information) and 594 and 633 nm for 3B, 3C, and 3D complexes, Table 1.

## CONCLUSIONS

We have successfully applied accelerated aging and ball milling for the synthesis of several types of heteroleptic complexes of Pd(II) containing azobenzenes and phosphines, despite the fact that their formation requires a series of complex molecular modifications during the reaction. The high efficiency, use of solvent in catalytic amounts, low-energy input as well as simplicity in processing and handling reactants and products render these two solid-state synthetic methods as excellent alternatives to solvent-based synthesis. Described results, which are consistent with the objectives of green chemistry, open up the possibilities to much wider application of accelerated aging and ball milling for synthesis of elaborate molecular systems.

This preliminary investigation clearly demonstrated a strong influence of triphenylphosphine and 1,1'-bis-(diphenylphosphino)ferrocene as ancillary ligands on the photophysical properties of dipalladated azobenzenes. In comparison with initial dipalladated 4-dimethylamino-4'-nitroazobenzene complex 3, the presence of phosphines in new complexes coupled with appropriate 4,4'-substituents on the azobenzene ligand and Pd...Pd interactions in the bridged complexes significantly enhance fluorescence at room temperature in solid state for complexes 3A, 3B, 3C, and 3D or in solution for complexes 3A, 3C, and 3D. Thus, the Pd(II) heteroleptic complexes with azobenzenes and phosphines could be utilized in designing new emitters.

## EXPERIMENTAL SECTION

**General Measurements.** All chemicals were used as supplied, and the reactions were carried out under aerobic condition. Electronic absorption spectra were recorded in  $\text{CHCl}_3$  at 25 °C with a thermostatted cell compartment. Fluorescence spectra were recorded in  $\text{CHCl}_3$  at 25 °C. Fluorescence in the solid-state was detected at 25

°C by confocal microscope using nujol mull of samples with appropriate excitation wavelengths.

**NMR Measurements.** The  $^1\text{H}$  and  $^{31}\text{P}$  NMR spectra in solution were recorded at 25 °C in  $\text{CDCl}_3$  at 600.13 MHz for the  $^1\text{H}$  and 242.92 MHz for the  $^{31}\text{P}$  resonances. The  $^{31}\text{P}$  NMR spectra were externally referenced using 85%  $\text{H}_3\text{PO}_4$ , Table S1 (Supporting Information).  $^1\text{H}$  signal assignment was based on the chemical shifts and quantum chemical calculations of the chemical shifts.

$^{31}\text{P}$  MAS NMR spectra of solid samples were recorded on 300 MHz NMR spectrometer equipped with 5 mm Magic Angle Probe, Table S1 (Supporting Information). Larmor frequency of phosphorus nuclei was 122.65 MHz. The  $^{31}\text{P}$  MAS NMR spectra were externally referenced using  $\text{AlPO}_4$ , which was set to  $-29.5$  ppm corresponding to 85%  $\text{H}_3\text{PO}_4$  ( $\delta$  0.0 ppm). All samples were spun at the magic angle with ca. 5 kHz spinning frequency. Repetition delay in all experiments was 30 s; the number of scans was between 168 and 3760.

**Single-Crystal X-ray Measurements.** Measurements were performed on X-ray diffractometers with microfocus Cu or Mo tubes at room temperature. Program package CrysAlisPRO<sup>15</sup> was used for data reduction. The structures were solved using SHELXS97<sup>16</sup> and refined with SHELXL97.<sup>16</sup> Models were refined using the full-matrix least-squares refinement. Hydrogen atoms were treated as riding entities using the command AFIX in SHELXL-97.<sup>16</sup> Molecular geometry calculations were performed by PLATON,<sup>17</sup> and molecular graphics were prepared using ORTEP-3<sup>18</sup> and CCDC-Mercury.<sup>19</sup> Crystallographic and refinement data for the structures reported in this paper are shown in Table S2 (Supporting Information).

**Powder X-ray Diffraction (PXRD) Experiments.** Experiments were performed on X-ray diffractometer with Cu  $K\alpha_1$  (1.54056 Å) radiation at 40 mA and 40 kV. The scattered intensities were measured with a scintillation counter. The angular range was from 3° to 50° ( $2\theta$ ) with steps of 0.02°, and the measuring time was 1 s per step. The data collection and analysis was performed using the program package Philips X'Pert. Details about the solving and the refinement of the structure for 1C and 1D are given in the Supporting Information.

**ESI Mass Spectrometry.** ESI mass spectra were recorded on a mass spectrometer working in the positive mode. The compounds were dissolved in  $\text{CHCl}_3$  to obtain a concentration of approximately  $10^{-4}$  mol/dm<sup>3</sup>. Stock solution was diluted with MeOH to approximately  $10^{-5}$  mol/dm<sup>3</sup> and injected into the ESI source. Helium was used as a collision gas. Expected natural abundance isotope cluster patterns for various ion clusters were calculated with the ICR-2LS program.<sup>20</sup>

**Computational Methods.** The computations were performed with Gaussian09,<sup>21</sup> using B3LYP functional<sup>22</sup> and two basis sets. Geometry optimization was done with SDD pseudopotential and accompanying basis<sup>23</sup> on Pd atoms and 6-31G(d,p) basis on all other atoms. NMR shifts and excited states were calculated with the extended SDD basis on Pd by additional s, p, d and f functions,<sup>24</sup> while 6-311+G(d,p) basis was used on all other atoms. In the latter calculations solvated state was accounted by the PCM model<sup>25</sup> with chloroform as a solvent. NMR shifts were calculated by the GIAO formalism<sup>26</sup> and the lowest 32 excited singlet states by the time dependent DFT method (TD-DFT).

**Aging Reactions.** In all aging reactions the mixture of solid reactants prepared by gentle grinding in an agate mortar and put in a small test tube underwent a chemical reaction upon exposure to acetone vapors at room temperature. The reactions were carried out in a sealed vessel (100 mL volume) filled with air and acetone vapors. The mixture of solid reactants was kept in acetone vapors for 48 (1A–3A, 1B–3B) or 72 (1C–3C, 1D–3D) hours. Analysis of the products using PXRD revealed complete conversion of reactants into the products. Initial complexes (DMF) $\text{PdCl}(\mu\text{-R}^1\text{C}_6\text{H}_3\text{N}=\text{NC}_6\text{H}_3\text{R}^2)\text{-PdCl}(\text{DMF})$  1–3 were prepared as described previously.<sup>9a,27</sup>

**1A.** The reaction was carried out with 55.52 mg (0.091 mmol) of 1 and 47.73 mg (0.182 mmol) of tpp. Isolated yield: 98.0% (88.15 mg). Found: C 57.98, H 4.02, N 2.78. Calcd. for  $\text{C}_{48}\text{H}_{38}\text{N}_2\text{P}_2\text{Pd}_2\text{Cl}_2$ : C 58.32, H 3.87, N 2.83. UV-vis ( $\text{CHCl}_3$ )  $\lambda_{\text{max}}/\text{nm}$  ( $\epsilon/10^4 \text{ M}^{-1} \text{ cm}^{-1}$ ): 305 (1.40), 345 (1.25), 395 (0.78), 466 (0.30). (+)ESI-MS  $m/z$  (rel.

int., %):  $[\text{Pd}_2\text{Cl}(\text{L1-2H})(\text{tpp})_2]^+$  953.0 (100);  $[\text{Pd}_2\text{Cl}_2(\text{L1-2H})(\text{tpp})_2+\text{NaCl}]^+$  1044.9 (2).

**2A.** 53.18 mg (0.083 mmol) of **2** and 43.58 mg (0.166 mmol) of tpp. Isolated yield: 98.5% (83.35 mg). Found: C 57.77, H 4.11, N 2.52. Calcd. for  $\text{C}_{49}\text{H}_{40}\text{N}_2\text{O}_2\text{P}_2\text{Pd}_2\text{Cl}_2$ : C 57.78, H 3.96, N 2.75. UV-vis ( $\text{CHCl}_3$ )  $\lambda_{\text{max}}/\text{nm}$  ( $\epsilon/10^4 \text{ M}^{-1} \text{ cm}^{-1}$ ): 349 (0.71), 393 (0.62), 460 (0.43). (+)ESI-MS  $m/z$  (rel. int., %):  $[\text{Pd}_2\text{Cl}(\text{L2-2H})(\text{tpp})_2]^+$  983.1 (100);  $[\text{Pd}_2\text{Cl}_2(\text{L2-2H})(\text{tpp})_2+\text{NaCl}]^+$  1075.0 (13).

**3A.** 52.35 mg (0.075 mmol) of **3** and 39.33 mg (0.150 mmol) of tpp. Isolated yield: 99.0% (79.91 mg). Found: C 56.02, H 4.11, N 4.91. Calcd. for  $\text{C}_{50}\text{H}_{42}\text{N}_4\text{O}_2\text{P}_2\text{Pd}_2\text{Cl}_2$ : C 55.78, H 3.93, N 5.20. UV-vis ( $\text{CHCl}_3$ )  $\lambda_{\text{max}}/\text{nm}$  ( $\epsilon/10^4 \text{ M}^{-1} \text{ cm}^{-1}$ ): 300 (2.24), 384 (0.78), 542 (3.96). (+)ESI-MS  $m/z$  (rel. int., %):  $[\text{Pd}_2\text{Cl}(\text{L3-2H})(\text{tpp})_2]^+$  1041.1 (100);  $[\text{Pd}_2\text{Cl}_2(\text{L3-2H})(\text{tpp})_2+\text{NaCl}]^+$  1133.0 (5).

**1B.** 33.25 mg (0.054 mmol) of **1** and 57.17 mg (0.218 mmol) of tpp. Isolated yield: 99.0% (81.62 mg). Found: C 66.98, H 4.66, N 1.88. Calcd. for  $\text{C}_{84}\text{H}_{68}\text{N}_2\text{P}_4\text{Pd}_2\text{Cl}_2$ : C 66.68, H 4.53, N 1.85. (+)ESI-MS  $m/z$  (rel. int., %):  $[\text{Pd}_2\text{Cl}(\text{L1-2H})(\text{tpp})_2]^+$  953.0 (100);  $[\text{Pd}_2\text{Cl}_2(\text{L1-2H})(\text{tpp})_2+\text{NaCl}]^+$  1044.9 (17);  $[\text{Pd}_2\text{Cl}(\text{L1-2H})(\text{tpp})_3]^+$  1214.9 (7).

**2B.** 31.22 mg (0.049 mmol) of **2** and 51.17 mg (0.195 mmol) of tpp. Isolated yield: 98.6% (74.21 mg). Found: C 66.47, H 4.92, N 1.86. Calcd. for  $\text{C}_{85}\text{H}_{70}\text{N}_2\text{O}_2\text{P}_2\text{Pd}_2\text{Cl}_2$ : C 66.16, H 4.57, N 1.82. (+)ESI-MS  $m/z$  (rel. int., %):  $[\text{Pd}_2\text{Cl}(\text{L2-2H})(\text{tpp})_2]^+$  983.1 (100);  $[\text{Pd}_2\text{Cl}_2(\text{L2-2H})(\text{tpp})_2+\text{NaCl}]^+$  1075.1 (3).

**3B.** 30.55 mg (0.044 mmol) of **3** and 45.91 mg (0.175 mmol) of tpp. Isolated yield: 99.4% (69.64 mg). Found: C 64.75, H 4.71, N 3.34. Calcd. for  $\text{C}_{86}\text{H}_{72}\text{N}_4\text{O}_2\text{P}_2\text{Pd}_2\text{Cl}_2$ : C 64.51, H 4.53, N 3.50. (+)ESI-MS  $m/z$  (rel. int., %):  $[\text{Pd}_2\text{Cl}(\text{L3-2H})(\text{tpp})_2]^+$  1041.1 (100);  $[\text{Pd}_2\text{Cl}_2(\text{L3-2H})(\text{tpp})_2+\text{NaCl}]^+$  1133.0 (2).

**1C.** 54.25 mg (0.089 mmol) of **1** and 49.29 mg (0.089 mmol) of dppf. Isolated yield: 98.8% (89.46 mg). Found: C 54.73, H 3.74, N 2.67. Calcd. for  $\text{C}_{46}\text{H}_{36}\text{N}_2\text{P}_2\text{FePd}_2\text{Cl}_2$ : C 54.25, H 3.56, N 2.75. UV-vis ( $\text{CHCl}_3$ )  $\lambda_{\text{max}}/\text{nm}$  ( $\epsilon/10^4 \text{ M}^{-1} \text{ cm}^{-1}$ ): 325 (1.54), 460 (0.40), 488 sh (0.36). (+)ESI-MS  $m/z$  (rel. int., %):  $[\text{Pd}_2\text{Cl}(\text{L1-2H})(\text{dppf})]^+$  983.0 (100);  $[\text{Pd}_2\text{Cl}(\text{L1-2H})(\text{dppfOH})]^+$  1000.0 (17);  $[\text{Pd}_4\text{Cl}_2(\text{L1-2H})_2(\text{dppf})_3]^{2+}$  1260.0 (21).

**2C.** 51.20 mg (0.080 mmol) of **2** and 44.34 mg (0.080 mmol) of dppf. Isolated yield: 99.2% (83.18 mg). Found: C 53.41, H 3.33, N 2.28. Calcd. for  $\text{C}_{47}\text{H}_{38}\text{N}_2\text{O}_2\text{P}_2\text{FePd}_2\text{Cl}_2$ : C 53.85, H 3.65, N 2.67. UV-vis ( $\text{CHCl}_3$ )  $\lambda_{\text{max}}/\text{nm}$  ( $\epsilon/10^4 \text{ M}^{-1} \text{ cm}^{-1}$ ): 361 (1.26), 474 (0.59). (+)ESI-MS  $m/z$  (rel. int., %):  $[\text{Pd}_2\text{Cl}(\text{L2-2H})(\text{dppf})]^+$  1013.0 (51);  $[\text{Pd}_2\text{Cl}(\text{L2-2H})(\text{dppfOH})]^+$  1030.0 (100);  $[\text{Pd}_4\text{Cl}_2(\text{L2-2H})_2(\text{dppf})_3]^{2+}$  1290.0 (4).

**3C.** 50.44 mg (0.072 mmol) of **3** and 40.05 mg (0.072 mmol) of dppf. Isolated yield: 99.0% (79.13 mg). Found: C 52.49, H 3.16, N 4.97. Calcd. for  $\text{C}_{48}\text{H}_{40}\text{N}_4\text{O}_2\text{P}_2\text{FePd}_2\text{Cl}_2$ : C 52.11, H 3.64, N 5.06. UV-vis ( $\text{CHCl}_3$ )  $\lambda_{\text{max}}/\text{nm}$  ( $\epsilon/10^4 \text{ M}^{-1} \text{ cm}^{-1}$ ): 300 (2.05), 347 sh (1.18), 425 (0.80), 564 (2.78). (+)ESI-MS  $m/z$  (rel. int., %):  $[\text{Pd}_2\text{Cl}(\text{L3-2H})(\text{dppf})]^+$  1071.1 (91);  $[\text{Pd}_2\text{Cl}(\text{L3-2H})(\text{dppfOH})]^+$  1088.1 (100);  $[\text{Pd}_4\text{Cl}_2(\text{L3-2H})_2(\text{dppf})_3]^{2+}$  1348.1 (11).

**1D.** 38.38 mg (0.063 mmol) of **1** and 69.75 mg (0.126 mmol) of dppf. Isolated yield: 99.5% (98.44 mg). Found: C 60.97, H 4.36, N 1.69. Calcd. for  $\text{C}_{80}\text{H}_{64}\text{N}_2\text{P}_4\text{Fe}_2\text{Pd}_2\text{Cl}_2$ : C 61.10, H 4.10, N 1.78. UV-vis ( $\text{CHCl}_3$ )  $\lambda_{\text{max}}/\text{nm}$  ( $\epsilon/10^4 \text{ M}^{-1} \text{ cm}^{-1}$ ): 364 (1.13), 380 sh (1.01), 455 (0.13). (+)ESI-MS  $m/z$  (rel. int., %):  $[\text{Pd}_2\text{Cl}(\text{L1-2H})(\text{dppf})_2]^+$  1537.1 (100);  $[\text{Pd}_2\text{Cl}(\text{L1-2H})(\text{dppf})(\text{dppfOH})]^+$  1553.1 (4);  $[\text{Pd}_2\text{Cl}_2(\text{L1-2H})(\text{dppfOH})_2+\text{Na}]^+$  1629.0 (14);  $[\text{Pd}_4\text{Cl}_2(\text{L1-2H})_2(\text{dppf})_3]^{2+}$  1260.1 (3);  $[\text{Pd}_4\text{Cl}_4(\text{L1-2H})_2(\text{dppf})_3+\text{CH}_3\text{OH}+2\text{Na}]^{2+}$  1305.6 (1).

**2D.** 37.50 mg (0.058 mmol) of **2** and 64.95 mg (0.117 mmol) of dppf. Isolated yield: 99.1% (93.04 mg). Found: C 60.33, H 4.49, N 1.74. Calcd. for  $\text{C}_{81}\text{H}_{66}\text{N}_2\text{O}_4\text{Fe}_2\text{Pd}_2\text{Cl}_2$ : C 60.70, H 4.15, N 1.75. UV-vis ( $\text{CHCl}_3$ )  $\lambda_{\text{max}}/\text{nm}$  ( $\epsilon/10^4 \text{ M}^{-1} \text{ cm}^{-1}$ ): 382 (1.30), 483 (0.23). (+)ESI-MS  $m/z$  (rel. int., %):  $[\text{Pd}_2\text{Cl}(\text{L2-2H})(\text{dppf})_2]^+$  1567.1 (85);  $[\text{Pd}_2\text{Cl}(\text{L2-2H})(\text{dppf})(\text{dppfOH})]^+$  1585.2 (14);  $[\text{Pd}_2\text{Cl}_2(\text{L2-2H})(\text{dppfOH})_2+\text{Na}]^+$  1659.0 (25);  $[\text{Pd}_4\text{Cl}_2(\text{L2-2H})_2(\text{dppf})_3]^{2+}$  1290.0 (100);  $[\text{Pd}_4\text{Cl}_4(\text{L2-2H})_2(\text{dppf})_3+\text{CH}_3\text{OH}+2\text{Na}]^{2+}$  1335.6 (69).

**3D.** 35.60 mg (0.051 mmol) of **3** and 56.53 mg (0.102 mmol) of dppf. Isolated yield: 98.9% (83.74 mg). Found: C 58.98, H 4.38, N 3.33. Calcd. for  $\text{C}_{82}\text{H}_{68}\text{N}_4\text{O}_4\text{Fe}_2\text{Pd}_2\text{Cl}_2$ : C 59.30, H 4.13, N 3.37.

UV-vis ( $\text{CHCl}_3$ )  $\lambda_{\text{max}}/\text{nm}$  ( $\epsilon/10^4 \text{ M}^{-1} \text{ cm}^{-1}$ ): 307 (2.24), 541 (1.99). (+)ESI-MS  $m/z$  (rel. int., %):  $[\text{Pd}_2\text{Cl}(\text{L3-2H})(\text{dppf})_2]^+$  1625.2 (100);  $[\text{Pd}_2\text{Cl}(\text{L3-2H})(\text{dppf})(\text{dppfOH})]^+$  1641.2 (7);  $[\text{Pd}_2\text{Cl}_2(\text{L3-2H})(\text{dppfOH})_2+\text{Na}]^+$  1717.2 (5);  $[\text{Pd}_4\text{Cl}_2(\text{L3-2H})_2(\text{dppf})_3]^{2+}$  1348.1 (45);  $[\text{Pd}_4\text{Cl}_4(\text{L3-2H})_2(\text{dppf})_3+\text{CH}_3\text{OH}+2\text{Na}]^{2+}$  1394.1 (7).

**Ball-Milling Reactions.** All complexes were obtained by analogous ball-milling reactions with the same ratio of azobenzenes and the initial Pd complex. Complexes **1A** and **3A** were prepared by liquid-assisted grinding (LAG) as described previously.<sup>6</sup>

Grinding experiments were performed at room temperature in a 10 mL stainless steel jar using two 7 mm stainless steel grinding balls. A grinder mill operating at 25 Hz frequency was used for the synthesis. All LAG reactions were performed according to recently reported procedure for complexes **1A** and **3A**<sup>6</sup> using 30  $\mu\text{L}$  of acetone (or nitromethane) in each reaction. PXRD experiments revealed complete conversion of reactants into the products after 30 (**1A** and **3A**), 60 (**2A**, **2C** and **3C**), and 90 (**1B–3B**, **1D–3D**) minutes of grinding. Elemental analysis results of all complexes are in good agreement with the calculated values (data given in the Supporting Information).

## ■ ASSOCIATED CONTENT

### Supporting Information

Procedures for the mechanochemical and solvent-based reactions; PXRD patterns of reactants and products for all experiments; X-ray crystallographic data (CIF) for CCDC 975112–975114; details of molecular and crystal structure of **2A** and **3B**; crystallographic data collection and structure refinement data; details about the solving and the refinement of the structure for **1C** and **1D**; <sup>31</sup>P NMR spectra of all complexes (in  $\text{CHCl}_3$  and MAS); calculated geometries and energies of isomers of complexes; UV-vis spectra and the complete list of the computed excited states. This material is available free of charge via the Internet at <http://pubs.acs.org>.

## ■ AUTHOR INFORMATION

### Corresponding Author

\*E-mail: [curic@irb.hr](mailto:curic@irb.hr).

### Notes

The authors declare no competing financial interest.

## ■ ACKNOWLEDGMENTS

The Ministry of Science, Education and Sports of the Republic of Croatia provided financial support for this research (Grant No. 098-0982915-2950, 098-0982904-2953, and 119-1193079-3069). Computations were done on the Isabella cluster at SRCE, Zagreb. The authors thank the European Commission for access to SLONMR (EU FP7 Project “East-NMR”, Grant No. 228461), and ARRS (Grant No. P1-242). Authors would like to acknowledge Prof. Robert E. Dinnebier and Dr. Dubravka Šišak for support in the structure determinations from powder diffraction data, Miha Friedrich and Aleksandar Gačša for help with the NMR measurements, Dr. Primož Šket for valuable discussions, and Dr. Snježana Kazazić for help with the ESI-MS measurements.

## ■ REFERENCES

- (1) (a) James, S. L.; Adams, C. J.; Bolm, C.; Braga, D.; Collier, P.; Friščić, T.; Grepioni, F.; Harris, K. D. M.; Hyett, G.; Jones, W.; Krebs, A.; Mack, J.; Maini, L.; Orpen, A. G.; Parkin, I. P.; Shearouse, W. C.; Steed, J. W.; Waddell, D. C. *Chem. Soc. Rev.* **2012**, *41*, 413–447. and references therein. (b) Friščić, T. *Chem. Soc. Rev.* **2012**, *41*, 3493–3510.
- (2) (a) Užarević, K.; Halasz, I.; Đilović, I.; Bregović, N.; Rubčić, M.; Matković-Čalogović, D.; Tomišić, V. *Angew. Chem., Int. Ed.* **2013**, *52*, S504–S508. (b) Friščić, T.; Halasz, I.; Beldon, P. J.; Belenguer, A. M.;

- Adams, F.; Kimber, S. A. J.; Honkimäki, V.; Dinnebier, R. E. *Nat. Chem.* **2013**, *5*, 66–73. (c) Bučar, D.-K.; Day, G. M.; Halasz, I.; Zhang, G. G. Z.; Sander, J. R. G.; Reid, D. G.; MacGillivray, L. R.; Duer, M. J.; Jones, W. *Chem. Sci.* **2013**, *4*, 4417–4425. (d) Braga, D.; Maini, L.; Grepioni, F. *Chem. Soc. Rev.* **2013**, *42*, 7638–7648. (e) Štrukil, V.; Igrc, M. D.; Eckert-Maksić, M.; Friščić, T. *Chem.—Eur. J.* **2012**, *18*, 8464–8473. (f) Stolle, V.; Szuppa, T.; Leonhardt, S. E. S.; Ondruschka, B. *Chem. Soc. Rev.* **2011**, *40*, 2317–2329. (g) Friščić, T.; Reid, D. G.; Halasz, I.; Stein, R. S.; Dinnebier, R. E.; Duer, M. J. *Angew. Chem., Int. Ed.* **2010**, *49*, 712–715. (h) Kuroda, R.; Yoshida, J.; Nakamura, A.; Nishikori, S. *CrystEngComm* **2009**, *11*, 427–432. (i) Declerck, V.; Nun, P.; Martinez, J.; Lamaty, F. *Angew. Chem., Int. Ed.* **2009**, *48*, 9318–9321. (j) Garay, A. L.; Pichon, A.; James, S. L. *Chem. Soc. Rev.* **2007**, *36*, 846–855. (k) Imai, Y.; Tajima, N.; Sato, T.; Kuroda, R. *Org. Lett.* **2006**, *8*, 2941. (l) Etter, M. C.; Reutzler, S. M.; Choo, C. G. *J. Am. Chem. Soc.* **1993**, *115*, 4411–4412.
- (3) (a) Friščić, T.; Halasz, I.; Strobridge, F. C.; Dinnebier, R. E.; Stein, R. S.; Fabian, L.; Curfs, C. *CrystEngComm* **2011**, *13*, 3125–3129. (b) Chen, P.-N.; Lai, C.-C.; Chiu, S.-H. *Org. Lett.* **2011**, *13*, 4660–4663. (c) Braga, D.; Grepioni, F. *Angew. Chem., Int. Ed.* **2004**, *43*, 4002–4011. (d) Belcher, W. J.; Longstaff, C. A.; Neckenig, M. R.; Steed, J. W. *Chem. Commun.* **2002**, 1602–1603.
- (4) (a) Andre, V.; Braga, D.; Grepioni, F.; Duarte, M. T. *Cryst. Growth Des.* **2009**, *11*, 5108–5116. (b) Schartman, R. R. *Int. J. Pharm.* **2009**, *365*, 77–80. (c) Shan, N.; Zaworotko, M. J. *Drug Discovery* **2008**, *13*, 440–446. (d) Trask, A. V.; Haynes, D. A.; Motherwell, W. D. S.; Jones, W. *Chem. Commun.* **2006**, 51–53.
- (5) (a) Mottillo, C.; Lu, Y.; Pham, M.-H.; Cliffe, M. J.; Do, T.-O.; Friščić, T. *Green Chem.* **2013**, *15*, 2121–2131. (b) Cliffe, M. J.; Mottillo, C.; Bučar, D.-K.; Friščić, T. *Chem. Sci.* **2012**, *3*, 2495–2500. (c) Cinčić, D.; Brekalo, I.; Kaitner, B. *Chem. Commun.* **2012**, *48*, 11683–11685. (d) Braga, D.; Grepioni, F.; Maini, L.; Prosperi, S.; Gobetto, R.; Chierotti, M. R. *Chem. Commun.* **2010**, *46*, 7715–7717. (e) Užarević, K.; Rubčić, M.; Đilović, I.; Kokan, Z.; Matković-Čalোগović, D.; Cindrić, M. *Cryst. Growth Des.* **2009**, *9*, 5327–5333. (f) Braga, D.; Giuffreda, S. L.; Grepioni, F.; Chierotti, M. R.; Gobetto, R.; Palladino, G.; Polito, M. *CrystEngComm* **2007**, *9*, 879–881. (g) Nakamatsu, S.; Toyota, S.; Jones, W.; Toda, F. G. *Chem. Commun.* **2005**, 3808–3810.
- (6) Cinčić, D.; Juribašić, M.; Babić, D.; Molčanov, K.; Šket, P.; Plavec, J.; Čurić, M. *Chem. Commun.* **2011**, *47*, 11543–11545.
- (7) (a) Chen, Z.-N.; Zhao, N.; Fan, Y.; Ni, J. *Coord. Chem. Rev.* **2009**, *253*, 1–20. (b) Cooke, M. W.; Hanan, G. S. *Chem. Soc. Rev.* **2007**, *36*, 1466–1476. (c) Dupont, J.; Consorti, C. S.; Spencer, J. *Chem. Rev.* **2005**, *105*, 2527–2572.
- (8) (a) Snelders, D. J. M.; Van Koten, G.; Klein Gebbink, R. J. M. *Chem.—Eur. J.* **2011**, *17*, 42–57. (b) Albrecht, M. *Chem. Rev.* **2010**, *110*, 576–623. (c) Van der Boom, M. E.; Milstein, D. *Chem. Rev.* **2003**, *103*, 1759–1792. (d) Albrecht, M.; Van Koten, G. *Angew. Chem., Int. Ed.* **2001**, *40*, 3750–3781.
- (9) (a) Juribašić, M.; Budimir, A.; Kazazić, S.; Čurić, M. *Inorg. Chem.* **2013**, *52*, 12749–12757. (b) Juribašić, M.; Čurić, M.; Molčanov, K.; Matković-Čalогоović, D.; Babić, D. *Dalton Trans.* **2010**, *39*, 8769–8778.
- (10) Štepanička, P.; Cisarova, I.; Schulz, J. *Organometallics* **2011**, *30*, 4393–4403.
- (11) (a) Agrawal, D.; Zins, E.-L.; Schröder, D. *Chem.—Asian J.* **2010**, *5*, 1667–1676. (b) Qian, R.; Liao, Y.-X.; Guo, Y.-L.; Guo, H. *J. Am. Soc. Mass Spectrom.* **2006**, *17*, 1582–1589.
- (12) (a) Adrio, L.; Antelo, J. M.; Ortigueira, J. M.; Fernandez, J. J.; Fernandez, A.; Pereira, M. T.; Vila, J. M. *J. Organomet. Chem.* **2009**, *694*, 1273–1282. (b) Ye, J.; Chen, W.; Wang, D. *Dalton Trans.* **2008**, 4015–4022. (c) Lopez-Tores, M.; Fernandez, A.; Fernandez, J. J.; Suarez, A.; Pereira, M. T.; Ortigueira, J. M.; Vila, J. M.; Adams, H. *Inorg. Chem.* **2001**, *40*, 4583–4587. (d) Vila, J. M.; Pereira, M. T.; Ortigueira, J. M. *Organometallics* **1999**, *18*, 5484–5487. (e) Garrone, R.; Romano, A. M.; Santi, R.; Millini, R. *Organometallics* **1998**, *17*, 4519–4522. (f) Plowman, R. A.; Power, L. F. *J. Aust. Chem.* **1971**, *24*, 303–308. (g) Plowman, R. A.; Power, L. F. *J. Aust. Chem.* **1971**, *24*, 309–316.
- (13) (a) Diez, A.; Fornies, J.; Garcia, A.; Lalinde, E.; Moreno, M. T. *Inorg. Chem.* **2005**, *44*, 2443–2453. (b) Vicente, J.; Areas, A.; Bautista, D.; Jones, P. G. *Organometallics* **1997**, *16*, 2127–2138. (c) Vicente, J.; Chichote, M. T.; Lagunas, M. C.; Jones, P. G.; Bembek, E. *Organometallics* **1994**, *13*, 1243–1250. (d) Rüttmann, S.; Williams, A. F.; Bernardinelli, G. *Angew. Chem., Int. Ed.* **1993**, *32*, 392–394.
- (14) (a) Ghedini, M.; Aiello, I.; Crispini, A.; Golemme, A.; La Deda, M.; Pucci, D. *Coord. Chem. Rev.* **2006**, *250*, 1373–1390. (b) Wu, Q.; Hook, A.; Wang, S. *Angew. Chem., Int. Ed.* **2000**, *39*, 3933–3935. (c) Lai, S. W.; Cheung, T. C.; Chan, M. C. W.; Cheung, K. K.; Peng, S. M.; Che, C. M. *Inorg. Chem.* **2000**, *39*, 255–262. (d) Van Houten, K. A.; Heath, D. C.; Barringer, C. A.; Rheingold, A. L.; Pilato, R. S. *Inorg. Chem.* **1998**, *37*, 4647–4653. (e) Neve, F.; Crispini, A.; Campagna, S. *Inorg. Chem.* **1997**, *36*, 6150–6156.
- (15) *CrysAlisPRO*; Oxford Diffraction, Ltd.: Oxford, U.K., 2007.
- (16) Sheldrick, G. M. *SHELXL97, Program for Refinement of Crystal Structures*; Universität Göttingen: Göttingen, Germany, 1997.
- (17) Spek, A. L. *PLATON98: A Multipurpose Crystallographic Tool*, 120398 Version; University of Utrecht: Utrecht, Netherlands, 1998.
- (18) Farrugia, L. J. *J. Appl. Crystallogr.* **1997**, *30*, 565–576.
- (19) McCabe, P.; Pidcock, E.; Shields, G. P.; Taylor, R.; Towler, M.; Macrae, C. F.; Edgington, P. R.; Van de Streek, J. *J. Appl. Crystallogr.* **2006**, *39*, 453–457.
- (20) Anderson, G. A.; Bruce, J. E.; Smith, R. D. *ICR-2LS*, ver. 2.18; Pacific Northwest National Laboratory: Richland, WA, 1996.
- (21) Frisch, M. J.; Trucks, G. W.; Schlegel, H. B.; Scuseria, G. E.; Robb, M. A.; Cheeseman, J. R.; Scalmani, G.; Barone, V.; Mennucci, B.; Petersson, G. A.; Nakatsuji, H.; Caricato, M.; Li, X.; Hratchian, H. P.; Izmaylov, A. F.; Bloino, J.; Zheng, G.; Sonnenberg, J. L.; Hada, M.; Ehara, M.; Toyota, K.; Fukuda, R.; Hasegawa, J.; Ishida, M.; Nakajima, T.; Honda, Y.; Kitao, O.; Nakai, H.; Vreven, T.; Montgomery, J. A., Jr.; Peralta, J. E.; Ogliaro, F.; Bearpark, M.; Heyd, J. J.; Brothers, E.; Kudin, K. N.; Staroverov, V. N.; Kobayashi, R.; Normand, J.; Raghavachari, K.; Rendell, A.; Burant, J. C.; Iyengar, S. S.; Tomasi, J.; Cossi, M.; Rega, N.; Millam, N. J.; Klene, M.; Knox, J. E.; Cross, J. B.; Bakken, V.; Adamo, C.; Jaramillo, J.; Gomperts, R.; Stratmann, R. E.; Yazyev, O.; Austin, A. J.; Cammi, R.; Pomelli, C.; Ochterski, J. W.; Martin, R. L.; Morokuma, K.; Zakrzewski, V. G.; Voth, G. A.; Salvador, P.; Dannenberg, J. J.; Dapprich, S.; Daniels, A. D.; Farkas, Ö.; Foresman, J. B.; Ortiz, J. V.; Cioslowski, J.; Fox, D. J. *Gaussian 09*, Revision D.01; Gaussian, Inc.: Wallingford, CT, 2009.
- (22) (a) Becke, A. D. *J. Chem. Phys.* **1993**, *98*, 5648–5652. (b) Lee, C.; Yang, W.; Parr, R. G. *Phys. Rev. B* **1988**, *37*, 785–789.
- (23) Andrae, D.; Haussermann, U.; Dolg, M.; Stoll, H.; Preuss, H. *Theor. Chim. Acta* **1990**, *77*, 123–141.
- (24) Zeizinger, M. J.; Burda, V.; Spooner, J.; Kapsa, V.; Leszczynski, J. *J. Phys. Chem. A* **2001**, *105*, 8086–8092.
- (25) Tomasi, J.; Mennucci, B.; Cancès, E. *J. Mol. Struct.: THEOCHEM* **1999**, *464*, 211–226.
- (26) Wolinski, K.; Hilton, J. F.; Pulay, P. *J. Am. Chem. Soc.* **1990**, *112*, 8251–8260.
- (27) (a) Babić, D.; Čurić, M.; Molčanov, K.; Ilc, G.; Plavec, J. *Inorg. Chem.* **2008**, *47*, 10446–10454. (b) Čurić, M.; Babić, D.; Višnjevac, A.; Molčanov, K. *Inorg. Chem.* **2005**, *44*, 5975–5977.